Elongation of confined ferrofluid droplets under applied fields

S. Banerjee,[1] M. Fasnacht,[1] S. Garoff,[1,2] and M. Widom[1]

[1]*Department of Physics, Carnegie Mellon University, Pittsburgh, Pennsylvania 15213*
[2]*Colloids, Polymers, and Surfaces Program, Carnegie Mellon University, Pittsburgh, Pennsylvania 15213*

Ferrofluids are strongly paramagnetic liquids. We study the behavior of ferrofluid droplets confined between two parallel plates with a weak applied field parallel to the plates. The droplets elongate under the applied field to reduce their demagnetizing energy and reach an equilibrium shape where the magnetic forces balance against the surface tension. This elongation varies logarithmically with aspect ratio of droplet thickness to its original radius, in contrast to the behavior of unconfined droplets. Experimental studies of a ferrofluid-water-surfactant emulsion confirm this prediction. [S1063-651X(99)00210-X]

I. INTRODUCTION

Ferrofluids [1] are oil- or water-based colloidal suspensions of permanently magnetized particles. In an applied magnetic field, the particles align, creating a strong paramagnetic response in the ferrofluid. Because they are fluids, these suspensions can flow in response to forces. For example, ferrofluid droplets elongate parallel to applied fields [2–7] and undergo tip-sharpening transitions [8,9]. When a ferrofluid droplet is confined between two plates in a ''thin film'' geometry, surrounded by an immiscible fluid, and a field is applied perpendicular to the plates, it undergoes field-induced bifurcations [10] leading to intricate labyrinthine patterns [11]. Ferrofluid emulsions [12] undergo structural transitions under an applied field from a randomly dispersed structure of the emulsion droplets to droplet chains, columns, and wormlike structures [13,14] depending on volume fraction, sample geometry, and the rate of field application.

We are interested in the elongation of ferrofluid droplets under applied magnetic fields. While the elongation of freely suspended, three-dimensional droplets has been well analyzed and observed [2–5], the elongation of droplets in the thin film geometry still remains relatively unstudied. In this geometry droplets are surrounded by an immiscible fluid and are confined between parallel plates (see Fig. 1) such that the thickness between the plates is much smaller than its undeformed diameter. The applied field is parallel to the plates. We calculate the elongation of the thin film droplets as a function of various parameters of the problem. Prior studies of ferrofluid droplets in this geometry [6,7] have considered droplet elongation under applied field and its use as a tool for measuring surface tension between the ferrofluid and the surrounding immiscible fluid.

A droplet of ferrofluid elongates under an applied field because of the demagnetizing fields of magnetic poles on the surface of the droplet. Surface poles arise wherever the droplet magnetization has a component perpendicular to the surface. The demagnetizing field that they create opposes the magnetization, creating a demagnetizing energy that depends on the shape of the droplet. The droplet elongates to reduce its demagnetizing field and energy. Because elongation increases the surface energy of the system, an equilibrium shape is reached when the magnetic forces balance against the surface tension forces.

In the case of freely suspended three-dimensional droplets the elongation can be calculated assuming that the droplets are ellipsoidal in shape for small elongation. The demagnetizing field is thus uniform and the elongation (major axis minus minor axis divided by minor axis) is found to be proportional to the undeformed droplet radius. The case of droplets confined in the thin film geometry, however, is more complex as it involves two length scales, droplet thickness and its undeformed diameter. In the limit of small aspect ratio (droplet thickness divided by its undeformed diameter) the demagnetizing fields are nonuniform. They are stronger near the edge of the droplet and fall off as $1/r$ away from the edge into the bulk of the droplet. Due to this $1/r$ falloff of the field we find that the elongation divided by droplet thickness is proportional to the logarithm of the aspect ratio. This improves on the existing theory [6] which assumes that the demagnetizing field is uniform. We also perform an experiment which supports our predicted logarithmic behavior.

Section II of this paper presents our theoretical study of the elongation of a ferrofluid droplet confined within a thin film. Our principal result is a predicted logarithmic dependence of elongation on droplet aspect ratio. We contrast this result with the corresponding elongation of unconfined droplets. Section III describes an experiment done with ferrofluid emulsions that tests our theory. The experiment is in quali-
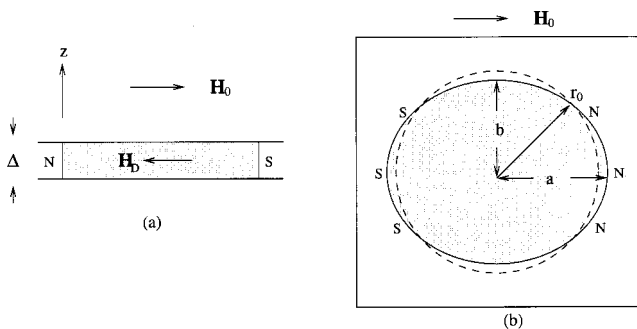

FIG. 1. (a) A side view of a ferrofluid droplet confined between two glass plates. (b) A top view of a ferrofluid droplet elongating under applied field. The dashed line shows the undeformed droplet. N and S indicate the north and south magnetic poles. $\mathbf{H}_D$ is the demagnetizing field.

tative agreement with our theoretical prediction, but differs quantitatively in at least one respect. In Sec. IV we discuss possible explanations of the discrepancy.

II. THEORY

Consider a paramagnetic liquid droplet confined in a thin film between two parallel plates with a gap Δ in the $\hat{z}$ direction (see Fig. 1). An immiscible liquid surrounds the droplet. Let the thickness Δ be much smaller than the radius of the undeformed droplet, r_0. This small aspect ratio

$$p = \frac{\Delta}{2r_0} \tag{1}$$

provides the pseudo-two-dimensional character of the problem. If a uniform, weak, field $\mathbf{H}_0$ is applied parallel to the plate, the droplet magnetizes. The magnetization creates an opposing demagnetizing field whose strength depends on the droplet shape. The droplet elongates to decrease its magnetic energy, reaching equilibrium when the magnetic forces balance against the restoring forces due to surface tension. In this section we define the elongation of the droplet and calculate the surface energy E_S and the magnetic energy E_M of the droplet as a function of its elongation. By minimizing the total energy with respect to the elongation we obtain the elongation as a function of $\mathbf{H}_0$, r_0, and Δ.

For simplicity assume the elongated droplet has a uniform cross section $\mathcal{C}$, independent of z. This corresponds to a contact angle of 90° between the paramagnetic liquid, the surrounding fluid, and the glass plates, and a plate spacing much less than the capillary length of the two liquids. Thus the droplet has straight edges if viewed from the side (see Fig. 1). The role of the contact angle will be discussed later in Sec. IV. We write the equation for $\mathcal{C}$ in polar coordinates as a generic smooth perturbation to a circle,

$$r = \alpha_1 + \alpha_2 \cos 2\theta. \tag{2}$$

We only include a single harmonic, since we expect coefficients for the higher harmonics to be much smaller than α_2 for small perturbations. The cross section $\mathcal{C}$ has semimajor axis a, and semiminor axis b [see Fig. 1(b)], with $\alpha_1 = (a+b)/2$ and $\alpha_2 = (a-b)/2$. We define the elongation of the droplet

$$\epsilon \equiv \frac{a}{b} - 1. \tag{3}$$

We assume that the elongation, ϵ, is much less than 1. Imposing the constraint that the volume of the droplet (Δ times cross-sectional area) remains constant we calculate

$$\alpha_1 = \frac{r_0}{(1+k^2/2)^{1/2}}, \quad \alpha_2 = \frac{r_0 k}{(1+k^2/2)^{1/2}}, \tag{4}$$

where $k = \epsilon/(2+\epsilon)$.

The surface energy is the sum of interfacial areas times surface tensions between all pairs of the three phases (solid glass, ferrofluid droplet, and immiscible fluid). For the case of uniform cross-section (90° contact angle) droplets, the glass-ferrofluid and glass–immiscible-fluid interfacial areas

are independent of the shape of $\mathcal{C}$ due to the fixed volume constraint. Hence we concern ourselves with the droplet-surfactant solution interface, the area of which is Δ times the perimeter. The perimeter of cross section $\mathcal{C}$ can be calculated as a power series in ϵ,

$$S = 2\pi r_0 \left(1 + \frac{3}{16}\epsilon^2 + O(\epsilon^3) \right). \tag{5}$$

As expected, the leading correction to S is second order in ϵ since the perimeter should increase regardless of the sign of ϵ. The relevant surface energy of the droplet is

$$E_s = \sigma_{FI} S \Delta, \tag{6}$$

where σ_{FI} is the surface tension of the ferrofluid–immiscible-fluid interface.

The total magnetic energy of any paramagnetic body under applied field is [15]

$$E_M = -\frac{1}{2} \int_V d^3\mathbf{r} \, \mathbf{H}_0 \cdot \mathbf{M}(\mathbf{r}). \tag{7}$$

The magnetization $\mathbf{M}(\mathbf{r})$ is determined by the self-consistent equation

$$\mathbf{M}(\mathbf{r}) = \chi[\mathbf{H}_0 + \mathbf{H}_D(\mathbf{r})] \tag{8}$$

for linear susceptibility χ, where

$$\mathbf{H}_D(\mathbf{r}) = \int_s d^2\mathbf{r}' [\mathbf{M}(\mathbf{r}') \cdot \hat{\mathbf{n}}(\mathbf{r}')] \frac{\mathbf{r} - \mathbf{r}'}{|\mathbf{r} - \mathbf{r}'|^3}$$
$$+ \int_V d^3\mathbf{r}' [\nabla \cdot \mathbf{M}(\mathbf{r}')] \frac{\mathbf{r} - \mathbf{r}'}{|\mathbf{r} - \mathbf{r}'|^3} \tag{9}$$

is the demagnetizing field due to the magnetization $\mathbf{M}(\mathbf{r})$, with $\hat{\mathbf{n}}(\mathbf{r}')$ being the outward normal at any point on the surface. The surface integral gives the demagnetizing field due to the surface poles which appear wherever the magnetization has a component normal to the surface. The volume integral gives the contribution to the demagnetizing field due to volume charges which appear at points where the magnetization has nonzero divergence.

To calculate the magnetic energy we expand $\mathbf{M}$ and $\mathbf{H}_D$ in power series in the susceptibility χ,

$$\mathbf{M}(\mathbf{r}) = \mathbf{M}^{(1)}(\mathbf{r}) + \mathbf{M}^{(2)}(\mathbf{r}) + \mathbf{M}^{(3)}(\mathbf{r}) + \cdots, \tag{10}$$

$$\mathbf{H}_D(\mathbf{r}) = \mathbf{H}_D^{(1)}(\mathbf{r}) + \mathbf{H}_D^{(2)}(\mathbf{r}) + \mathbf{H}_D^{(3)}(\mathbf{r}) + \cdots, \tag{11}$$

where $\mathbf{M}^{(n)}(\mathbf{r})$ and $\mathbf{H}_D^{(n)}(\mathbf{r})$ are proportional to χ^n. Equating terms in Eq. (8) of equal order in χ we get

$$\mathbf{M}^{(1)}(\mathbf{r}) = \chi \mathbf{H}_0 \tag{12}$$

and

$$\mathbf{M}^{(n+1)}(\mathbf{r}) = \chi \mathbf{H}_D^{(n)}(\mathbf{r}). \tag{13}$$

Note that $\mathbf{M}^{(1)}(\mathbf{r})$ is independent of $\mathbf{r}$ because the applied field is uniform whereas $\mathbf{M}^{(n)}(\mathbf{r})$ may depend on $(\mathbf{r})$ for n

>1 because $\mathbf{H}_D(\mathbf{r})$ may be nonuniform. To second order in χ we write the magnetic energy of the droplet in Eq. (7) as

$$E_M = -\tfrac{1}{2}\chi H_0^2 V - \tfrac{1}{2}\int_V d^3\mathbf{r}\,\mathbf{M}^{(1)}\cdot\mathbf{H}_D^{(1)}. \qquad (14)$$

The first term in Eq. (14) for the magnetic energy is independent of the shape of the droplet and hence unimportant for our consideration. The second term in the energy is the demagnetizing energy E_D due to a uniform magnetization $\mathbf{M}^{(1)} = \chi\mathbf{H}_0$. Because $\mathbf{M}^{(1)}$ is uniform there are no volume charges, and the surface poles appear only along the droplet–immiscible-fluid interface, to first order in χ. Rewrite the second term in Eq. (14) as an energy due to the induced surface charges along the curved surface of the droplet

$$E_D = \frac{1}{2}\chi^2\int_0^\Delta dz\int_0^\Delta dz'\oint ds\oint ds'\frac{(\hat{\mathbf{n}}\cdot\mathbf{H}_0)(\hat{\mathbf{n}}'\cdot\mathbf{H}_0)}{|\mathbf{r}-\mathbf{r}'|}. \qquad (15)$$

Here ds and ds' are infinitesimal arc lengths along the contour of the droplet $\mathcal{C}$, and $\hat{\mathbf{n}}$ and $\hat{\mathbf{n}}'$ are the outward normals to the curved surface of the droplet at points (s,z) and (s',z'), respectively.

Write $|\mathbf{r}-\mathbf{r}'| = \sqrt{R^2+(z-z')^2}$, where R is the in-plane distance between points at positions s and s' on $\mathcal{C}$. Integrating over z and z' in Eq. (15) yields [10]

$$E_D = \chi^2\Delta\oint ds\oint ds'(\hat{\mathbf{n}}\cdot\mathbf{H}_0)(\hat{\mathbf{n}}'\cdot\mathbf{H}_0)\Phi(R/\Delta), \quad (16)$$

where

$$\Phi(R/\Delta) = R/\Delta - \sqrt{1+(R/\Delta)^2}$$
$$+ \ln(R/\Delta)/[\sqrt{1+(R/\Delta)^2}-1]. \qquad (17)$$

Using Eq. (2) for $\mathcal{C}$ we calculate the demagnetizing energy in Eq. (16) as a series expansion in ϵ and the aspect ratio $p = \Delta/2r_0$,

$$E_D = \chi^2 H_0^2 V\left\{2p\ln\frac{B}{p} - 3\epsilon p\ln\frac{C}{p}+\cdots\right\}, \qquad (18)$$

where $V = \pi r_0^2\Delta$ is the volume of the droplet, and $B = 4e^{-1/2} = 2.43$ and $C = 4e^{-5/6} = 1.74$ are geometrical constants. The term in the brackets can be identified as 2π times the demagnetizing factor [15] of the droplet along the direction of applied field. Additional terms in the series in Eq. (18) are of higher order in ϵ or in p. For small elongation and small aspect ratio we may neglect these higher order terms.

Minimizing the total energy $E = E_S + E_M$ with respect to ϵ gives

$$\epsilon = \frac{\chi^2 H_0^2\Delta}{\sigma_{FI}}\ln\frac{C}{p}. \qquad (19)$$

Corrections to this result are higher order in aspect ratio p or higher order in ϵ itself. Interestingly, the elongation depends only logarithmically on the undeformed radius r_0, and has a much stronger dependence on the thickness Δ of the droplet.

This result differs from an earlier theory [6] which omits the logarithm because it assumes that the demagnetizing field is uniform inside the droplet.

In the case of unconfined, nearly ellipsoidal droplets [4,5], the demagnetizing field is quite uniform inside the droplet. The demagnetizing energy is therefore proportional to the volume $(\tfrac{4}{3}\pi r_0^3)$ of the droplet according to Eq. (14). The surface energy is proportional to the area $(4\pi r_0^2)$ and the elongation is thus proportional to r_0. In the case of thin film geometry, however, the demagnetizing field is very nonuniform. For distances much less than Δ near the droplet edge, the component of the demagnetizing field is of order M, since the edge acts like an infinite sheet of charge in the first approximation. For distances much greater than Δ the demagnetizing field is of order $M\Delta/r$, with r the distance away from the edge, since the edge acts as a line charge in this case. The contribution to the integral for the demagnetizing energy in Eq. (14) mainly comes from the bulk of the droplet and goes as $r_0\Delta^2\ln(r_0/\Delta)$. The surface energy is proportional to $2\pi r_0\Delta$ and the elongation is therefore proportional to $\Delta\ln(r_0/\Delta)$. The logarithmic variation of elongation with the aspect ratio is thus a signature of the nonuniform nature of the demagnetizing field inside the droplet.

III. EXPERIMENT

Setup

1. Sample preparation and structure

Our sample consisted of a ferrofluid–aqueous-solution emulsion confined between two glass plates. The oil-based ferrofluid used was EMG 905 made by Ferrofluidics with susceptibility $\chi = 1.9$ and saturation magnetization of 400 G [16]. To reduce the surface tension between the ferrofluid and the immiscible aqueous external phase, we incorporated surfactants in the aqueous phase. A solution of a commercial detergent made the best emulsions while solutions with other pure anionic surfactants either showed hardly any elongation of the ferrofluid droplets under an applied field or produced droplets without sharp boundaries with the aqueous phase. In contrast, our stable, well behaved emulsions allowed us to probe and confirm the fundamental aspects of our model.

To prepare the emulsions, a single drop of ferrofluid (~ 0.1 ml) was added to 10 ml of surfactant solution, which was a 12 times dilution of the commercial detergent. The liquid was shaken (by hand) to prepare the emulsion, creating ferrofluid droplets with diameters varying from ~ 5 to $200\ \mu$m. A small amount of this emulsion was then put between two glass plates which were circular, about 2 cm in diameter and 4 mm in thickness. These plates were cleaned using soap and alcohol and then rinsed with ROPure water. We also tried acid cleaning of the glass plates, however, it did not result in any noticeable change in the quality of the sample.

We used a rectangular spacer made of Mylar foil to separate the plates and prevent the emulsion from leaking out from the edges of the plates. The Mylar foil extended to the edges of the glass plates and had a rectangular hole in the center into which the emulsion was inserted. The thickness of a single Mylar spacer was measured to be $6.54 \pm 0.06\ \mu$m. The experiment was performed with one and
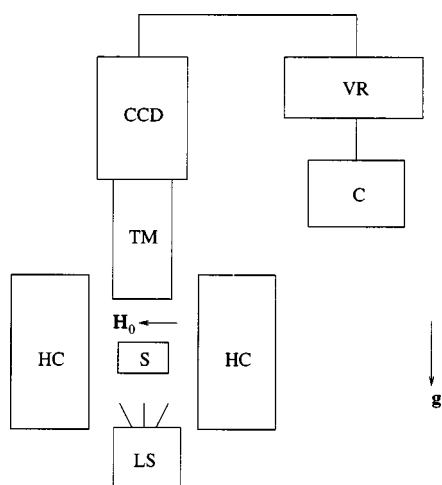
FIG. 2. A schematic diagram of the experimental setup. LS is the light source, HC is the Helmholtz coil, S is the sample, TM is the Tele-microscope, CCD is the CCD camera, VR is the video recorder, and C is the computer.

two spacers to ensure small aspect ratio.

For the cell assembly, the Mylar spacers were placed on the first plate and a drop of the emulsion was put in the center of the plate. The second plate was placed on top and the two plates were clamped together using a pair of brass rings. The rings were tightened by a set of four equally spaced screws. We measured the thickness variation across the sample by making a ''dry'' sample (without the emulsion) and counting resulting white light interference fringes. Although the thickness of Mylar spacers was measured to an accuracy of 1%, the thickness variation across the sample was found to be 10% resulting from the stresses due to clamping and possible entrapment of dust in the cell.

2. Apparatus

A schematic diagram of the experimental setup is shown in Fig. 2. We put the sample at the center of a pair of Helmholtz coils to ensure a homogeneous magnetic field. The field measured close to the sample using a Hall probe showed a variation of less than 4% across the sample. The sample was set up horizontally to prevent gravitational settling of the ferrofluid droplets. Horizontal alignment was achieved using a bubble level.

The sample was illuminated from below using a diffused light source and observed from above using a tele-microscope. The tele-microscope was connected to a charge-coupled device (CCD) camera and the image from it was fed into a video recorder and recorded on videotape. Images from the recording were later processed using *NIH Image*. We calibrated the optical system using a measuring reticule aligned along the two orthogonal directions of the CCD array. Figure 3 shows a low magnification view of a typical sample. The ferrofluid droplets appear much darker in the image than the surfactant solution around them.

3. Experimental procedure and image analysis

During the experiment the applied field was incremented every few seconds. We found the response of the droplets to the field to be nearly instantaneous and the shape of the
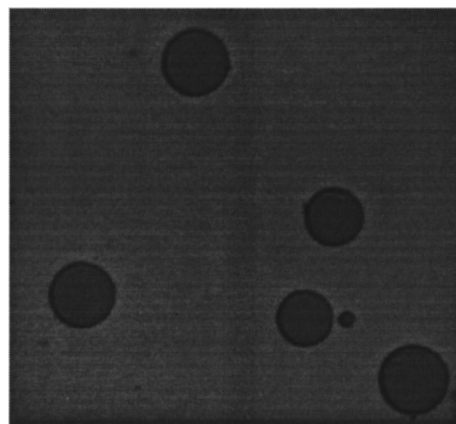

FIG. 3. A low magnification view of the sample showing ferrofluid droplets in emulsion.

droplets remained constant at constant field. Experiments with decreasing field strength showed no hysteresis in droplet shape. While droplet elongations were observed to be small we incremented the field in steps of about $1 G (10^{-4} T)$, and increased the increments up to about 5 G as the elongation increased. Droplet elongations appeared to vary smoothly with applied fields over the entire range from 0 to 50 G.

During each experiment the droplets were observed on a video monitor and recorded on tape. Figure 4 shows a droplet with $r_0 = 132.5 \, \mu m$ and $\Delta = 13.1 \, \mu m$ elongating under applied field at 50 G, typical of the highest field used in our experiment. After grabbing images of distorted droplets, we used a cutoff in pixel gray scale level to identify the droplet edge. The semimajor axis (a) and the semi-minor axis (b) were directly read off the image using *NIH Image*. At zero field measured elongations were small (rms magnitude around 0.003) and in random directions. These minor perturbations from a circular shape were likely due to microscopic distortion of the contact line pinned on weak surface heterogeneities. The ''observed radius'' r_0 was calculated as the average of the two semiaxes at zero field and the elongation at each field value was calculated using data analysis software.

4. Results

For each of the 48 droplets studied we plotted elongation ϵ, versus the square of the applied field, $\mathbf{H}_0$. Figure 5 shows
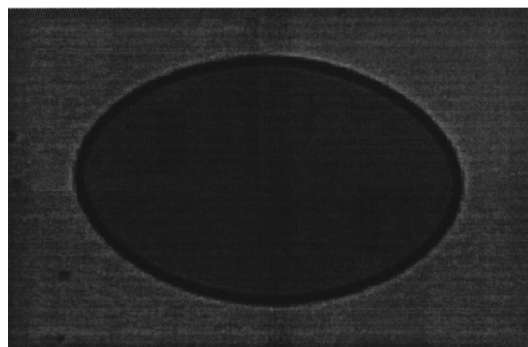

FIG. 4. A ferrofluid droplets with $r_0 = 132.5 \, \mu m$ and $\Delta = 13.1 \, \mu m$ elongating under an applied magnetic field of 50 G. The observed elongation is 0.56.
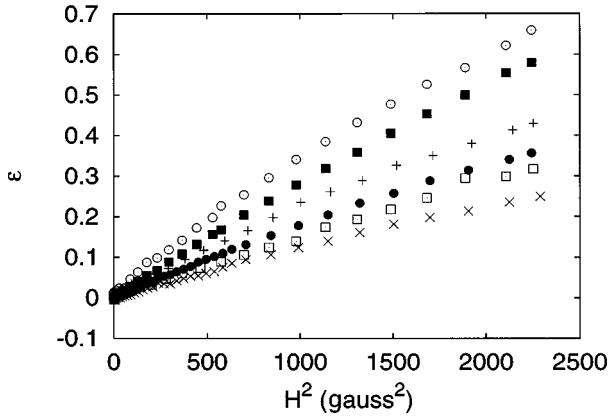
FIG. 5. The plot of elongation vs H^2 for droplets with different radii and two different thicknesses. The error bars are smaller than the size of the symbols on the plot. The symbols and radii for droplets with thickness spacing of $\Delta = 6.5$ μm are $\times$, 96.5 μm; $\bullet$, 112.0 μm, and $+$, 216.5 μm. The symbols and radii for droplets with thickness spacing of $\Delta = 13.1$ μm are $\boxdot$, 50.0 μm; $\blacksquare$, 98.0 μm; and $\odot$, 177.0 μm.

typical plots. The elongation is proportional to the square of the applied field for small applied fields as predicted. Saturation effects, although small, can be seen at higher values of the field. To compare the experimental data to our theoretical prediction (19), the plot of elongation for each droplet was fitted to

$$\frac{\epsilon}{\Delta} = k_0 + k_1 H_0^2 + k_2 H_0^4. \qquad (20)$$

We included terms only up to order H_0^4 because the saturation effects were observed to be small. We include k_0 to allow for the observed small elongations at zero field.

The coefficients k_1 of each droplet were then plotted versus the inverse of the aspect ratio $1/p = 2r_0/\Delta$ on a semilog plot (see Fig. 6). The theory predicts a slope of χ^2/σ_{FI} and an intercept of $1/C$ on the horizontal axis with $C = 1.74$. The data points in Fig. 6(a) fall on a straight line as predicted by the theory. Also, as predicted by the theory, the data points for two different droplet thicknesses overlay each other. There is substantial scatter in the data, but the deviations from a straight line are random and consistent with the error bars. The chief source of uncertainty was the 10% uncertainty in thickness due to the variation observed across the sample. Figure 6(b) displays the deviation of k_1 from the best fit normalized by the uncertainty. The uncertainties in measuring ϵ, r_0, and $\mathbf{H}_0$ were found to be negligible in comparison.

Dividing the susceptibility $\chi = 1.9$ for the ferrofluid used by the slope$ = 0.119 \pm 0.004$ cm/dyn obtained from the fitted line we get $\sigma_{FI} = 30.4 \pm 1.1$ dyn/cm, typical of oil-water surface tensions. From the fitted line we also get $C = 0.35 \pm 0.08$, differing substantially from our theoretically predicted value of 1.74. This discrepancy can be explained by considering the deviations from our two main assumptions of uniform magnetization and uniform cross section of the droplet. In the Discussion section below we explore the validity of our assumptions and the qualitative effect of any deviations from them to our result.
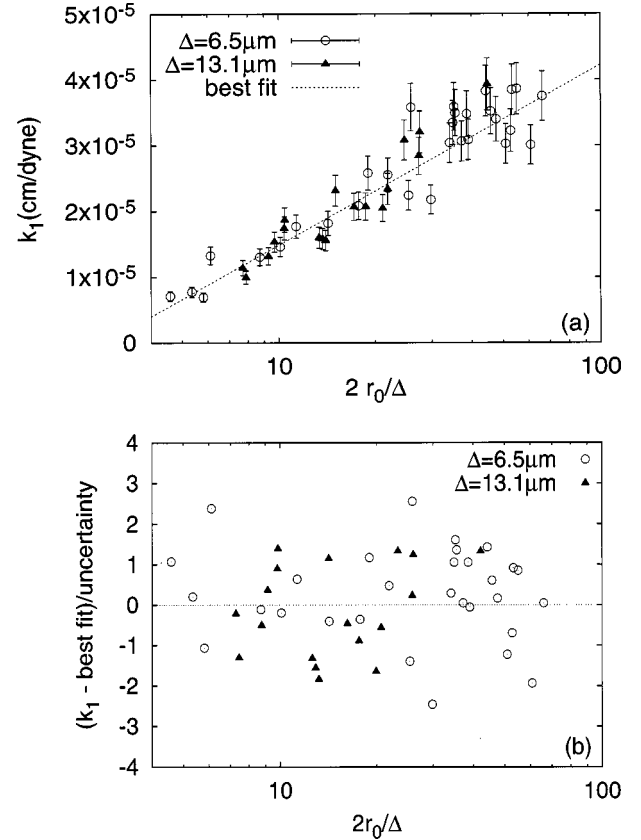

FIG. 6. (a) The plot of k_1 vs $1/p = (2r_0/\Delta)$ on a log scale. The dashed line is the best fit of the data to a straight line. (b) The deviation plot of the data from the best fit normalized by uncertainty of each data point.

In Fig. 7(a) we plot k_1 (the coefficient of H_0^2 in ϵ/Δ) versus $1/p = 2r_0/\Delta$ on a linear scale. If the demagnetizing field inside the droplet was uniform as in the case of unconfined droplets, the plot would be a straight line. However, the plot is clearly not a straight line and the deviations from the best fitted straight line are systematic [see Fig. 7(b)]. This further supports our theoretical result that the demagnetizing field inside a confined droplet is nonuniform and the elongation divided by thickness is proportional to the logarithm of the aspect ratio.

IV. DISCUSSION

The results discussed in Sec. III agree with our theoretical prediction (19) of logarithmic variation of ϵ/Δ as a function of $1/p = 2r_0/\Delta$. The predicted coefficient of the logarithm, $\chi^2 H_0^2/\sigma_{FI}$, is consistent with experimental observations. However, our theoretical value for C is $4e^{-5/6} = 1.74$, whereas the experimentally measured value for C is 0.35 ± 0.08. To explain this discrepancy we consider the validity of two main assumptions, uniform magnetization and contact angle of 90°. We explore, qualitatively, consequences of deviations from these assumptions.

In Sec. II we employ a perturbation expansion for small susceptibility. To lowest order, the magnetization $\mathbf{M} = \mathbf{M}^{(1)} = \chi\mathbf{H}_0$, which is constant. For our experiments the susceptibility of the ferrofluid used was large, causing strong demagnetizing fields near the edge of the droplet which, in
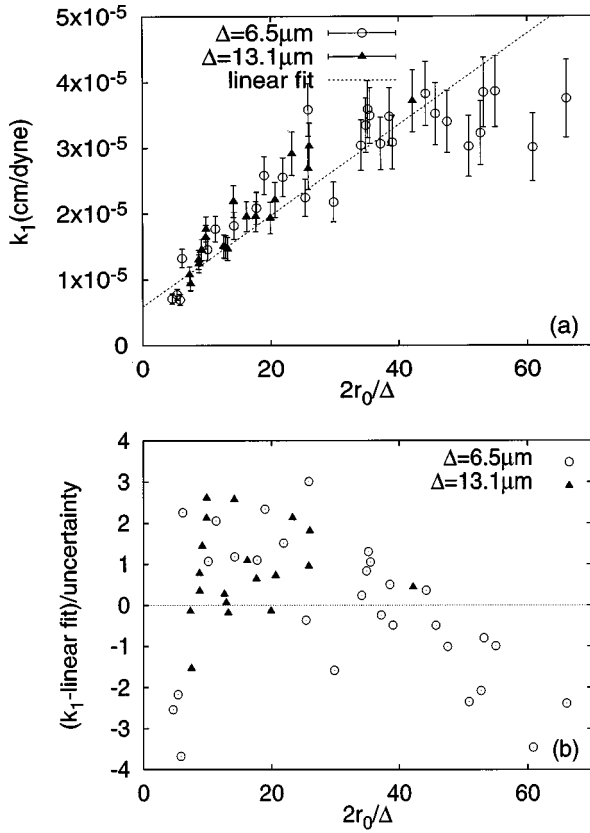
FIG. 7. (a) The plot of k_1 vs $1/p = 2r_0/\Delta$ and the best fit straight line. (b) The deviation plot of the data from the best linear fit.

turn, reduce the in-plane component of the magnetization and create an out-of-plane component of the magnetization near the edges. Consequently, the magnetic surface poles near the droplet edge spread out in a manner that reduces the magnetic energy E_M. We discuss this effect further in Sec. IV A.

We treated the case of contact angle $\beta = 90°$ between the glass plate and liquid droplet. The experiment, however, was performed with an oil-based ferrofluid in a surfactant solution for which the oil-glass contact angle $\beta < 90°$ (see Fig. 8). A contact angle of other than $90°$ redistributes the magnetic surface charges and changes interfacial areas. We consider these two effects in Secs. IV A and IV B, respectively. First, however, we address an ambiguity in the definition of aspect ratio and elongation which results from the nonuniformity of droplet cross section.

Our experiment observes the profile of the largest cross section of the droplet. For a circular droplet with $\beta < 90°$ this is the radius r_1 defined as the radius at midgap as shown in Fig. 8. For an elongated droplet we measure the semimajor and semiminor axes a_1 and b_1 and, through Eq. (3), the
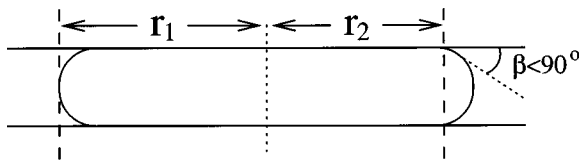

FIG. 8. A ferrofluid droplet making an acute contact angle with the glass plates.

elongation ϵ_1. We also define r_2, a_2, b_2, and ϵ_2 associated with the ferrofluid–immiscible–fluid–glass plate contact line. Since Δ is much less than the capillary length of the ferrofluid–immiscible fluid, to a good approximation [17] the profile of the droplet will be an arc of a circle, so the difference between r_1 and r_2 is of order Δ, and likewise for the semimajor and semiminor axes. The difference $\epsilon_1 - \epsilon_2$ is of order Δ/r_1 relative to the elongation. Recall that our result (19) for the elongation is only the lowest order term in a series expansion in the aspect ratio. Thus the distinction between r_1 and r_2, and between ϵ_1 and ϵ_2, does not alter our result at the lowest order in aspect ratio.

A. Corrections to magnetic energy

Our assumption of uniform magnetization is valid for small χ but for large χ strong demagnetizing fields reduce the in-plane component of the magnetization M_x and create an out-of-plane component M_z. This out-of-plane magnetization induces a charge density on the top and bottom surfaces of the droplet while the reduction of M_x removes some charge from the droplet edge. This charge redistribution necessarily reduces the energy E_M. Deviations of the contact angle from $90°$ affect the magnetic energy in a similar fashion because the inward or outward bulging spreads a given amount of surface charge over a slightly larger area. Charge redistribution reduces the values of the constants B and C in Eq. (18) but does not alter the coefficient of the logarithmic terms.

The coefficient of the logarithmic terms remains unchanged because the total charge within a distance of order Δ from a given point on the edge remains unchanged. Gauss's law relates the charge near the edge of the droplet to the magnetization in the bulk. Although the demagnetizing fields are strong near the edge they fall off as $1/r$ beyond a distance of order Δ from the edge. The magnetization in the bulk therefore remains uniform and equal to $\mathbf{M}^{(1)}$. Hence the total charge within a region of order Δ remains unchanged although it gets redistributed.

Now consider the origin of the order $Vp \ln p$ terms in Eq. (18). These terms arise because $\mathbf{H}_D$ falls off as $1/r$ far from the edge of the droplet. The $1/r$ falloff in $\mathbf{H}_D$ causes a $1/r$ variation in the deviation of $\mathbf{M}(\mathbf{r})$ from $\mathbf{M}^{(1)}$. After integrating over space as indicated in Eq. (7) this $1/r$ variation leads to a logarithm of the aspect ratio. Charge redistribution leaves the coefficient of the $1/r$ falloff unchanged because of the conservation of charge described above. Viewed from afar, the droplet edge remains effectively a line charge with a fixed linear charge density. Therefore the coefficient of the $Vp \ln p$ term is independent of the charge distribution.

In contrast, the order Vp terms in Eq. (18) depend upon details of the region close to the droplet edge. This is evident by considering the total volume within a distance Δ of the edge, estimated as an area Δ^2 times the circumference $2\pi r_0$. We consider, for the moment, the case $\epsilon = 0$. Since the droplet volume $V = \pi r_0^2 \Delta$, and $p = \Delta/2r_0$, we see that the volume near the edge is of order Vp. Surface magnetic poles create an energy density in this region of space, leading to an order Vp contribution to the demagnetizing energy that determines the value of the constant B. Since charge redistribution lowers the magnetic energy, the value of B is reduced.

A similar effect is observed in the self-energies of a current-carrying ribbon compared with a wire of circular cross section carrying the same current. The wire has a smaller self-energy because its current is distributed over a volume whereas the current is concentrated on a surface for the ribbon. The functional form of these self-energies is related to the demagnetization energy in Eq. (18). In particular, there are logarithmic terms whose coefficients depend on the total current but not on the current distribution, while the quantity equivalent to B is smaller for the wire than for the ribbon.

The demagnetization energy is always positive and decreases with elongation. A smaller demagnetization energy (due to smaller value of B) should exhibit weaker variation with respect to the elongation. Thus, we expect the value of C for a bulging droplet with non-uniform magnetization to be smaller than that for a straight-edged droplet with uniform magnetization. This effect may explain why the experimentally determined value of C is lower than the theoretically calculated value.

B. Corrections to surface energy

When the contact angle differs from 90°, the cross section of the droplet depends on z. Consequently, the contact areas of the glass plates with the droplet and with the surfactant solution may vary as the droplet elongates. All the three interfacial areas must be taken into account to calculate the surface energy. The total surface energy is

$$E_S = \sigma_{FI} A_C + 2\sigma_{FG} A_G + 2\sigma_{IG}(A - A_G), \quad (21)$$

where the three surface tensions between ferrofluid and immiscible fluid, ferrofluid and glass, and surfactant solution and glass, are denoted by σ_{FI}, σ_{FG}, and σ_{IG}, respectively, A_C and A_G are defined below, and the total area of the sample is denoted by A. The factors of 2 in the second and third terms of the surface energy account for the two glass surfaces.

The area of the droplet-surfactant solution interface A_C is given approximately by the circumference of C multiplied by the arc length of the bulge,

$$A_C = 2\pi r_1 \left(1 + \frac{3}{16}\epsilon^2\right) \Delta \frac{(\pi/2 - \beta)}{\cos\beta}. \quad (22)$$

We use r_1 here to calculate the circumference of the droplet because it is the radius observed during the experiment. To first order in the aspect ratio, using r_1 or r_2 in Eq. (22) yields the same result.

The droplet's contact area with the glass plates must be adjusted to maintain a constant total volume of ferrofluid as the droplet elongates. We approximate the volume of the bulging region by the circumference of C multiplied by the projected area of the bulge. The contact area A_G must be adjusted so that $A_G\Delta$ changes by the negative of the change in volume of the bulge. Thus we write

$$A_G = 2\pi r_2^2 \left[1 - \frac{3}{32}\left\{\frac{(\pi/2 - \beta)}{\cos^2\beta} - \tan\beta\right\}\frac{\Delta}{r_2}\epsilon^2\right]. \quad (23)$$

Using r_2 instead of r_1 makes the above result exact for zero elongation. The area of ferrofluid in contact with the glass plates decreases with elongation for an acute contact angle because the volume of the fluid contained in the outward bulge of the droplet increases and therefore the fluid contained in the bulk of the droplet decreases. For obtuse contact angles exactly the opposite happens for similar reasons.

Finally, consider how these corrections to magnetic and surface energies affect the elongation calculated in Eq. (19) for the case $\beta = 90°$ with uniform magnetization. The functional form of the magnetic energy (18) remains the same but the values of constants B and C are smaller. The ϵ dependence of the surface energy remains quadratic, but the coefficient now depends upon a linear combination of the three surface tensions σ_{FI}, σ_{FG}, and σ_{IG}. In our result for the elongation (19) the constant C will now have a value smaller than 1.74 and σ_{FI} will be replaced by a linear combination of the three surface tensions. For $\beta \neq 90°$ the experiment cannot be used to determine σ_{FS} unless σ_{FG} and σ_{IG} are known. Since β in general is not 90°, it is only possible to measure the effective surface tension during elongation, and not σ_{FI} itself.

V. CONCLUSIONS

We study the elongation ferrofluid droplets, confined in thin film geometry, under weak applied field. Our theoretical calculations predict the elongation of a droplet depends logarithmically on aspect ratio. This behavior contrasts with the case of unconfined three-dimensional droplets where elongation is directly proportional to undeformed droplet radius. We measured the elongation of ferrofluid droplets in an experiment performed on ferrofluid droplets in a ferrofluid-water-surfactant emulsion. The results of our experiment agree with the functional form of our theoretical prediction, however, the experimentally measured value of C differs from the predicted value. We suggest corrections due to high susceptibility and the droplet contact angle with the confining plates as a source of this discrepancy.

ACKNOWLEDGMENTS

[1] R. E. Rosensweig, *Ferrohydrodynamics* (Cambridge University Press, Cambridge, England, 1985).

[2] V. I. Arkhipenko, Y. D. Barkov, and V. G. Bashtovoi, Magnetohydrodynamics **14**, 373 (1978).

[3] V. I. Drozdova, T. V. Skrobotova, and V. V. Chekanov, Magnetohydrodynamics **15**, 16 (1979).

[4] J. C. Bacri and D. Salin, J. Phys. (France) Lett. **43**, 649 (1982).

[5] V. G. Bashtovoi, S. G. Pogirinitsakaya, and A. G. Reks, Magnetohydrodynamics **23**, 23 (1987).

[6] C. Flament, S. Lacis, J. C. Bacri, A. Cebers, S. Neveu, and R. Perzynski, Phys. Rev. E **53**, 4801 (1996).

[7] V. G. Bashtovoi *et al.* (unpublished, cited in Ref. [6]).

[8] J. C. Bacri and D. Salin, J. Phys. (France) Lett. **44**, 415 (1983).

[9] H. Li, T. C. Halsey, and A. Lobkovsky, Europhys. Lett. **27**, 575 (1994).

[10] S. A. Langer, R. E. Goldstein, and D. P. Jackson, Phys. Rev. A **46**, 4894 (1992).

[11] R. E. Rosensweig, M. Zahn, and R. Shumovich, J. Magn. Magn. Mater. **39**, 127 (1983).

[12] J. Bibette, D. Roux, and F. Nallet, Phys. Rev. Lett. **65**, 2470 (1990).

[13] J. Liu, E. M. Lawrence, A. Wu, M. L. Ivey, G. A. Flores, K. Javier, J. Bibette, and J. Richard, Phys. Rev. Lett. **74**, 2828 (1995).

[14] G. A. Flores *et al.*, Int. J. Mod. Phys. B **10**, 3283 (1996).

[15] W. F. Brown, *Magnetostatic Principles in Ferromagnetism* (North Holland, Amsterdam, 1962).

[16] Ferrofluidics, Inc. (private communication).

[17] A. W. Adamson, *Physical Chemistry of Surfaces* (Interscience, New York, 1967).